Effective Drug Delivery, *In Vitro* and *In Vivo*, by Carbon-Based Nanovectors Noncovalently Loaded with Unmodified Paclitaxel

Jacob M. Berlin,[†,¶] Ashley D. Leonard,[†,¶] Tam T. Pham,[†,¶] Daisuke Sano,[§,¶] Daniela C. Marcano,[†] Shayou Yan,[⊥] Stefania Fiorentino,[⊥] Zvonimir L. Milas,[§] Dmitry V. Kosynkin,[†] B. Katherine Price,[†] Rebecca M. Lucente-Schultz,[†] XiaoXia Wen,[∥] M. Gabriela Raso,[⊥] Suzanne L. Craig,[#] Hai T. Tran,[⊥] Jeffrey N. Myers,[§,*] and James M. Tour[†,‡,*]

[†]Department of Chemistry, and the [‡]Smalley Institute for Nanoscale Science and Technology, Rice University, MS-222, 6100 Main Street, Houston, Texas 77005, [§]Head and Neck Surgery, Unit 441, [⊥]Thoracic/Head and Neck Medical Oncology, [∥]Experimental Diagnostic Imaging, and [#]Department of Veterinary Medicine and Surgery, The University of Texas M.D. Anderson Cancer Center, 1515 Holcombe Boulevard, Houston, Texas 77030. [¶]These authors contributed equally to this work.

ABSTRACT Many new drugs have low aqueous solubility and high therapeutic efficacy. Paclitaxel (PTX) is a classic example of this type of compound. Here we show that extremely small (<40 nm) hydrophilic carbon clusters (HCCs) that are PEGylated (PEG-HCCs) are effective drug delivery vehicles when simply mixed with paclitaxel. This formulation of PTX sequestered in PEG-HCCs (PTX/PEG-HCCs) is stable for at least 20 weeks. The PTX/PEG-HCCs formulation was as effective as PTX in a clinical formulation in reducing tumor volumes in an orthotopic murine model of oral squamous cell carcinoma. Preliminary toxicity and biodistribution studies suggest that the PEG-HCCs are not acutely toxic and, like many other nanomaterials, are primarily accumulated in the liver and spleen. This work demonstrates that carbon nanomaterials are effective drug delivery vehicles *in vivo* when noncovalently loaded with an unmodified drug.

KEYWORDS: carbon nanotechnology · biodistribution · cancer · drug delivery · toxicity

An increasing number of drug candidates with high therapeutic efficacy have low water solubility, posing a challenge for *in vivo* delivery.[1] We are seeking to develop a safe, modular drug delivery platform that can be loaded with unmodified hydrophobic drugs and thereby enable their delivery. Ideally, in the future, it will be possible to continue to develop this modular platform into a targeted drug delivery vehicle. In this paper, we describe the initial step toward this goal by demonstration of a nontargeted platform that can sequester and deliver a hydrophobic drug.

Paclitaxel (PTX) is a classic example of a water-insoluble drug with high therapeutic efficacy. In the FDA-approved commercial formulation of PTX (Taxol, Bristol-Myers-Squibb, Princeton, NJ), the drug is solubilized in ethanol and a polyethoxylated castor oil, Cremophor EL (Cremophor). The use of Cremophor as the excipient for PTX is well-known to cause significant allergic reactions, including anaphylaxis. Consequently, patients are premedicated with antihistamines and corticosteroids in order to prevent potentially life-threatening hypersensitivity reactions.[2] One solution to this problem has been the sequestering of PTX in albumin, and the commercial formulation is called Abraxane.[3] Though milder, significant side effects remain, such as sensory neuropathy.[3] It is noteworthy that both commercial formulations of PTX involve the noncovalent sequestration of the unmodified drug, likely due to both the ease of preparing this class of formulations and the fact that covalently modifying the PTX can alter its efficacy. Numerous efforts have been made to find alternative excipients for PTX that would show increased drug-loading and would be nontoxic.[4,5] Many of these strategies incorporate PEG into the excipient either to provide solubility in aqueous solutions or to increase blood circulation time or even control the drug release profile.[6−8] Owing to its rich formulation history, widespread use, generic availability, and continued need for a still less toxic formulation, PTX was selected as the initial hydrophobic drug to evaluate for sequestration in our nanoparticles.

Nanovectors, nanoparticles capable of transporting and delivering one or more bioactive molecules, are an emerging class of drug delivery platforms.[9−11] Nanovectors have been prepared from a variety of

*Address correspondence to jmyers@mdanderson.org, tour@rice.edu.

Received for review May 5, 2010 and accepted July 14, 2010.

Published online August 3, 2010. 10.1021/nn100975c

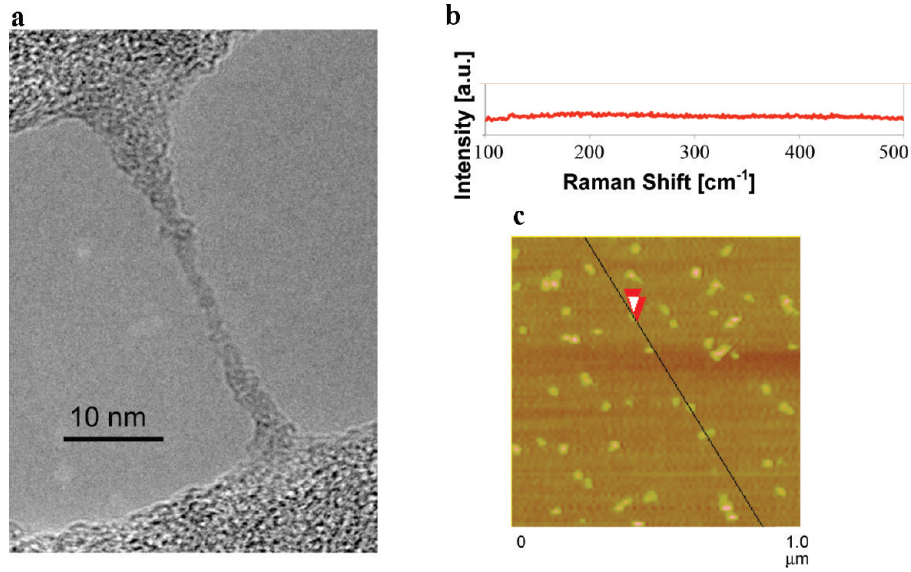

Figure 1. (a) TEM image of HCCs spanning an empty domain on a lacy carbon grid. The HCCs have aggregated during the sample preparation, which consisted of placing an aqueous dispersion of HCCs on the lacy carbon grid and drying the sample at 70 °C for 16 h. (b) Raman spectroscopy indicates that the HCCs have very few or no radial breathing modes. (c) AFM image of aggregated HCCs on mica. The overlapping red arrows indicate where the height of the HCCs was measured to be 1.9 nm.

materials and used to deliver a broad range of payloads, including siRNA and both hydrophilic and hydrophobic small molecules. Carbon nanomaterials, particularly those derived from carbon nanotubes, have received a great deal of attention as nanovectors.[12,13] In the majority of cases, the carbon nanomaterials are functionalized with PEG to provide solubility in aqueous solutions and increase blood circulation times. The predominant strategy for drug delivery using carbon nanovectors has been to covalently modify the drug with a linker that is then either covalently or noncovalently bound to the nanovector. This approach has been used for a variety of drugs, including carboranes,[14] cisplatin,[15] and PTX.[16,17] In pioneering work using single-walled carbon nanotubes (SWCNTs) to deliver PTX, branched PEG molecules, each with a long alkyl "tail", were functionalized with PTX molecules. These polymer conjugates were then bound to SWCNTs *via* the hydrophobic interaction between the alkyl tails and the nanotubes. *In vivo*, this formulation was more effective than

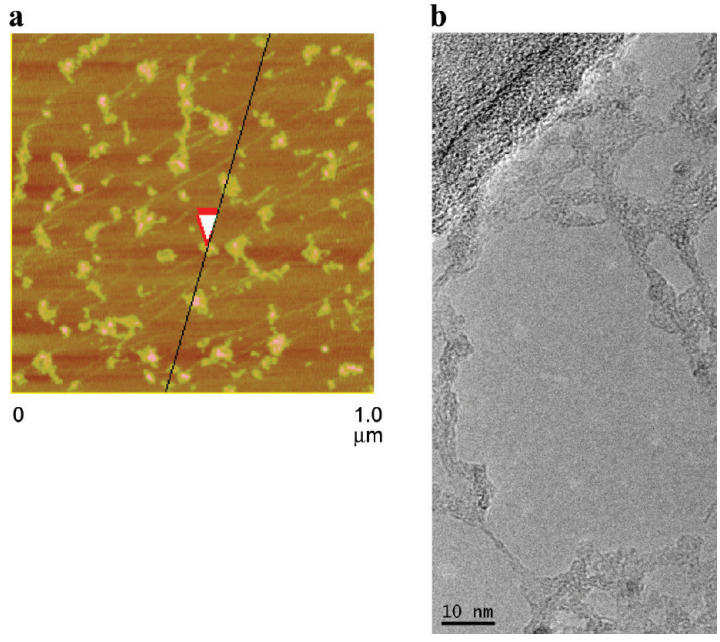

Figure 2. (a) AFM image of aggregated PEG-HCCs on mica. The overlapping red arrows indicate where the height of the PEG-HCCs was measured to be 1.7 nm. (b) TEM image of PEG-HCCs spanning an empty domain on a lacy carbon grid. The PEG-HCCs have aggregated during the sample preparation, which consisted of placing an aqueous solution of PEG-HCCs on the lacy carbon grid and drying the sample at 70 °C for 16 h.

Taxol, and the SWCNTs showed prolonged retention in the liver and spleen. Nonetheless, for all of the approaches mentioned, the requirement to covalently modify the drug presents a hurdle to adoption and retards the modularity of this class of formulations.

An alternative approach is to noncovalently load a nanovector with an unmodified drug molecule, such as PTX. This eliminates any concern about altering the drug's behavior and is a strategy that is easier to implement synthetically and is more modular. Probably the most well-established example of this strategy is liposomes,[18] where the drug is sequestered inside the particles. In some cases, this can be a limiting factor, as the drug is never or very poorly released from the liposomes.[19] There is a continuing interest in a variant of this strategy wherein hydrophobic drug molecules are sequestered on the hydrophobic surfaces of a nanovector. Carbon nanomaterials are a good choice for this approach as they are inherently hydrophobic. Several different carbon materials have been shown to successfully sequester hydrophobic compounds, including PTX.[20−27] These drug-loaded carbon nanomaterials have shown effective cell-killing *in vitro*, but to the best of our knowledge, there have been no reports of successful drug delivery *in vivo* using carbon nanomaterials loaded with unmodified drug molecules. Until this study, it remained an open question as to whether such formulations could prove effective in animal models.

Exploration of the potential toxicity and biodistribution of carbon nanomaterials is ongoing. Carbon is generally deemed nontoxic in simple forms, such as activated charcoal, and used for physisorption of organics in filters, water purification, and detoxifying formulations. Moreover, it has been observed that the body is able to clear foreign objects whose lengths are comparable to or less than the diameter of phagocytic cells (10−20 μm).[28] However, carbon nanostructures have attracted a great deal of attention and controversy over their potential toxicity. Recent reviews have highlighted the fact that early work on the toxicology of carbon nanomaterials has reached contradictory conclusions and raised more questions than it has answered.[29] A series of publications on the safety of carbon materials, wherein each paper was reviewed by a toxicologist along with a carbon materials scientist, came to the conclusion that "carbon nanomaterial samples are typically complex mixtures and ... that their toxicity depends on the specific formulation, in particular: (i) hydrophilicity ... (ii) metals content and bioavailability, and (iii) state of aggregation..."[30] In general, reduced toxicity is associated with structures that are hydrophilic, contain no trace metals, and cannot form fibrous aggregates that frustrate the phagocytic cells. Purified SWCNTs appear to have minimal toxicity and accumulate in the liver and spleen, with prolonged retention in those organs.[31,32] Even when extremely high doses of carbon nanomaterials are given intraperitoneally or orally, the mice remain healthy over an extended period of time.[33] Another recent study that modeled phagolysosomal conditions *in vitro* suggested that more highly oxidized carbon nanomaterials could be cleared more quickly by the liver than lesser oxidized carbon materials.[34]

Here we show that extremely small (<40 nm long) hydrophilic carbon clusters (HCCs) that are covalently modified with polyethylene glycol (PEG-HCCs) are effective drug delivery vehicles *in vitro* and *in vivo*. Drug loading is accomplished by simply mixing the nanovector PEG-HCCs with a hydrophobic drug; no covalent chemistry is required. No toxicity has been observed for the PEG-HCCs, and the drug-loaded formulation is highly stable.

RESULTS

Preparation and Characterization of HCCs and PEG-HCCs. HCCs were prepared from single-walled carbon nanotubes, which are 1 nm wide, by a previously described harsh oxidation procedure employing oleum and nitric acid (eq 1, only one of each functional group is shown for clarity).[35,36] In our previous reports on this procedure, we called the product ultrashort single-walled carbon nanotubes (US-SWCNT). In this previous report, radial breathing modes were observed in the Raman spectroscopy of the produced material, and tubular structures of 40−60 nm were observed by transmission electron microscopy (TEM).

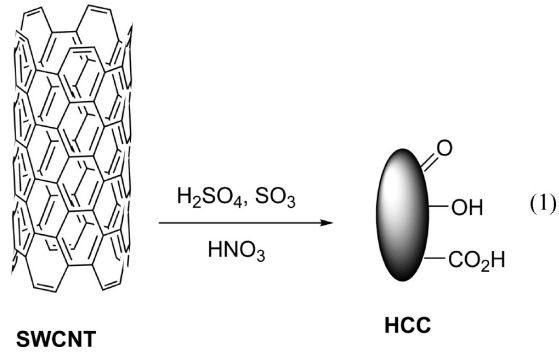

(1)

We have chosen to call the material produced for our current work HCCs rather than US-SWCNT because there are very few or no tubular structures observed in the TEM images (Figure 1a) and very few or no radial breathing modes observed by Raman spectroscopy (Figure 1b). The key difference between the previous report and our current work is the solubility of the starting SWCNTs in oleum, which is controlled by the catalyst concentration during their preparation.[37] A high catalyst concentration leads to shorter and less aggregated SWCNTs. The current procedure makes use of much more highly soluble SWCNTs (400 ppm) than the previous report (34 ppm). The increased solubility likely leads to better disentanglement and more complete oxidation, resulting in the smaller, less tubular HCCs. It is presumed that, due to the harsh oxidation conditions

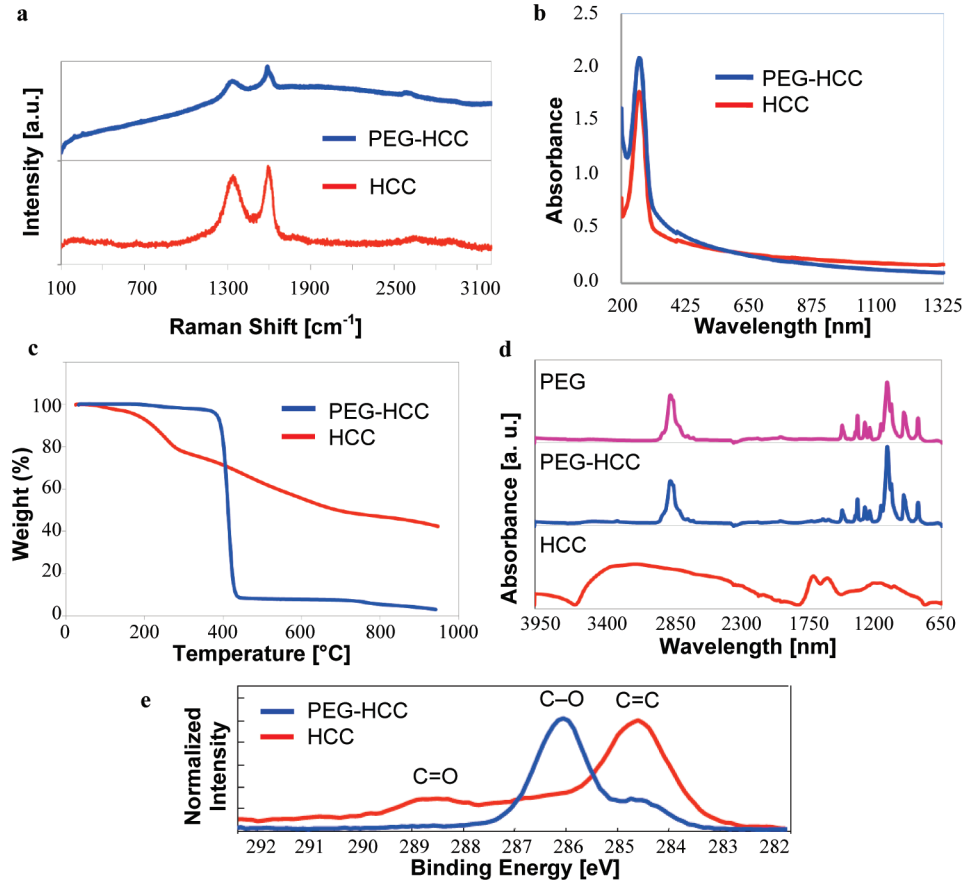

Figure 3. Characterization of HCCs and PEG-HCCs. (a) Raman spectra are free of radial breathing modes and have similar peak ratios. Fluorescence of the PEG-HCCs causes the baseline rise for that spectrum. (b) UV−vis spectra show similar traces for both compounds, indicative that their carbon cores are identical. (c) TGA indicates a 58% weight loss for the HCCs and a 97% weight loss for the PEG-HCCs (25−950 at 10 °C/min under Ar). (d) FTIR of HCCs, PEG-HCCs, and PEG alone shows the PEG's presence in the PEG-HCCs. The HCC absorbances are present but far less intense. (e) C(1s) portion of the XPS spectrum reflects both the high degree of oxidation for the HCCs (peaks >286 eV for C═O bonds) and the presence of the PEG polymer for the PEG-HCCs (strong peak at 286 eV for C−O bond).

employed, the surface of the HCCs is functionalized with a variety of oxygen-containing functionalities, such as alcohols, epoxides, ketones, and carboxylic acids. At a neutral pH of 7.0, HCCs have a ζ-potential of −29.97 mV. This is consistent with functionalization with carboxylic acids, which are deprotonated at neutral pH. Characterization by atomic force microscopy (AFM) indicated that the HCCs were beyond the resolution of the microscope, which has a tip scale of ~40 nm (Figure 1c). When the HCCs were analyzed by light scattering, a pH-dependent phenomenon was observed. Static light scattering indicated that at neutral pH the HCCs were 65 nm while at pH 14 they were 35 nm. Dynamic light scattering measurements were consistent with this trend. This behavior can be explained by aggregation that is controlled by the state of the oxygen functionalities on the HCCs. At neutral pH, some of the oxygen functionalities are protonated and some are deprotonated. Aggregation could be driven both by hydrophobic interactions between the remaining graphitic regions on the HCCs and hydrogen bonding between particles. At pH 14, all of the oxygen functionalities are deprotonated, making the particles highly negatively charged. Charge-based repulsion overwhelms any hydrophobic interaction, and the particles are individualized. On the basis of light scattering and AFM data, HCCs can be best described as <40 nm in length.

PEG-HCCs were prepared by coupling 5000 MW methoxy(polyethylene glycol) amine (mPEG-NH_2) to the carboxylic acids on the HCCs (eq 2, only one of each functional group is shown for clarity).[38] The PEG-HCCs were purified by sequential dialysis in DMF (2 days) and water (5 days) and then passage through a PD-10 desalting column to remove any coordinated metals or unbound PEG. PEG-HCCs had a ζ-potential of −23.04 mV.

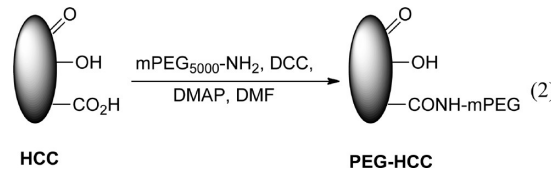

AFM analysis indicated that the PEG-HCCs appear to be more globular than the HCCs, which is likely the result of aggregation during sample preparation (Figure

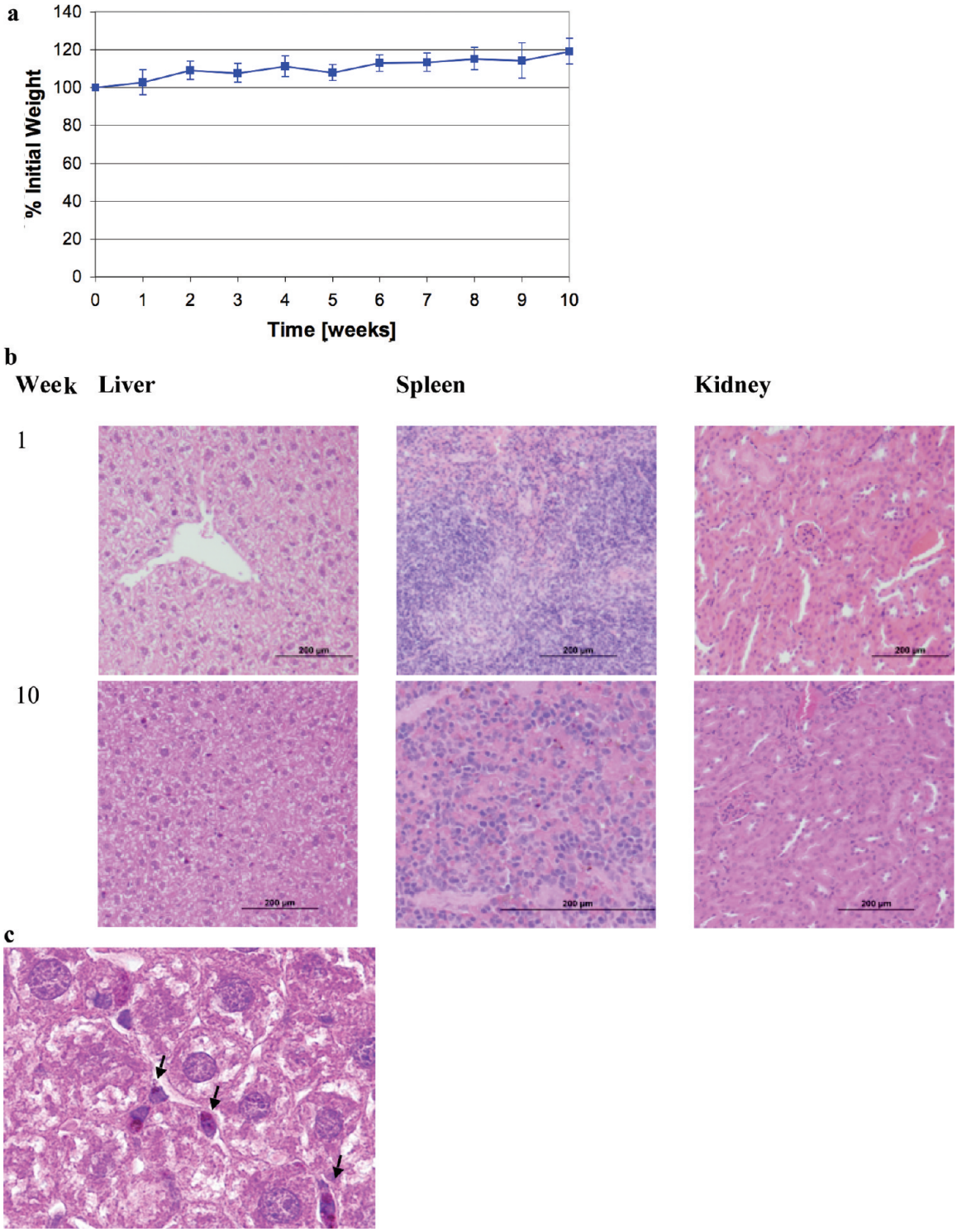

Figure 4. Toxicity study of PEG-HCCs given weekly for 10 weeks. (a) Average percent of initial weight of mice over the 10 week period. The mice gradually gained weight as is normal for healthy mice. (b) Samples of liver, spleen, and kidneys for mice treated for 1 week or 10 weeks. A few darker spots are evident in the liver sample of the mice treated for 10 weeks, but otherwise, the tissues appear normal. Scale bars are 200 μm. (c) Higher magnification (100×) image of the liver from a mouse treated for 10 weeks. The edge length of the image is 200 μm. The arrows mark the darker spots that likely indicate the presence of PEG-HCC aggregates.

2a). Indeed, in the TEM analysis, it was apparent that the PEG-HCCs could form extended structures when dried (Figure 2b). On the other hand, DLS indicated that at neutral pH the PEG-HCCs were below the limit of detection and are likely mostly individualized in solution and <50 nm. This individualization could result from the hydrophilic PEG shell preventing hydrophobic and hydrogen bonding interactions between the HCC cores.

Raman and UV−vis spectroscopy are very similar for the PEG-HCCs and HCCs, indicating that, as ex-

TABLE 1. Chemistry of Terminal Blood Samples for Analytes Related to Liver and Kidney Function.

time	AST (U/L)	ALT (U/L)	ALK PHOS (U/L)	bilirubin (mg/dL)	BUN (mg/dL)	serum creatine
1 wk ($n = 5$)	84 ± 16	41 ± 7	97 ± 12	0.16 ± 0.05	27.2 ± 4.0	<0.20
2 wk ($n = 5$)	97 ± 36	33 ± 6	75 ± 9	0.18 ± 0.05	22.5 ± 3.2	<0.20
4 wk ($n = 5$)	118 ± 52	64 ± 35	73 ± 7	0.20 ± 0.01	27.4 ± 2.3	<0.20
6 wk ($n = 5$)	148 ± 81	58 ± 29	55 ± 12	0.16 ± 0.05	16.7 ± 2.0	<0.20
8 wk ($n = 5$)	72 ± 15	30 ± 6	45 ± 11	0.10 ± 0.01	17.5 ± 1.8	<0.20
10 wk ($n = 5$)	61 ± 5	24 ± 3	39 ± 11	0.10 ± 0.01	16.9 ± 1.4	<0.20

TABLE 2. Additional Chemistry of Terminal Blood Samples.

time	sodium (mEg/L)	potassium (mEg/L)	chloride (mEg/L)	glucose (mg/dL)	calcium (mg/dL)
1 wk ($n = 5$)	152 ± 1	8.5 ± 0.9	109 ± 1	204 ± 77	12.0 ± 0.4
2 wk ($n = 5$)	153 ± 1	8.0 ± 0.7	113 ± 2	257 ± 35	11.5 ± 0.4
4 wk ($n = 5$)	152 ± 2	8.1 ± 0.5	113 ± 1	190 ± 18	10.7 ± 0.2
6 wk ($n = 5$)	153 ± 1	8.2 ± 0.9	113 ± 1	223 ± 15	10.8 ± 0.5
8 wk ($n = 5$)	149 ± 1	7.3 ± 0.4	113 ± 2	216 ± 40	10.5 ± 0.4
10 wk ($n = 5$)	153 ± 1	8.0 ± 1.0	112 ± 1	221 ± 47	10.4 ± 0.4

TABLE 3. Hematology Results for Terminal Blood Samples.

time	WBC ($\times 10^3/\mu L$)	RBC ($\times 10^6/\mu L$)	platelet count ($\times 10^3/\mu L$)	hemoglobin (g/dL)	hematocrit (%)	MCV (fL)	MCH (pg)	MCHC (g/dL)
1 wk ($n = 5$)	6.4 ± 1.4	8.9 ± 0.2	1543 ± 148	15.2 ± 0.5	50.5 ± 1.9	56.7 ± 1.6	17.1 ± 0.4	30.1 ± 0.4
2 wk ($n = 5$)	5.2 ± 0.4	9.1 ± 0.4	1290 ± 178	14.8 ± 0.4	49.2 ± 2.7	54.2 ± 1.1	16.4 ± 0.4	30.2 ± 0.9
4 wk ($n = 5$)	4.8 ± 0.5	8.7 ± 0.3	1329 ± 137	14.1 ± 0.4	44.8 ± 0.5	51.3 ± 2.0	16.1 ± 0.7	30.2 ± 0.9
6 wk ($n = 5$)	6.2 ± 1.6	8.6 ± 0.2	1415 ± 337	13.3 ± 0.2	44.5 ± 0.2	52.0 ± 1.3	15.6 ± 0.3	30.0 ± 0.3
8 wk ($n = 5$)	6.2 ± 2.2	8.3 ± 0.5	1609 ± 285	12.8 ± 0.8	42.1 ± 1.6	50.6 ± 1.2	15.3 ± 0.2	30.3 ± 0.8
10 wk ($n = 5$)	9.2 ± 1.4	8.9 ± 0.5	2149 ± 362	13.2 ± 0.8	44.6 ± 2.6	49.9 ± 0.9	14.9 ± 0.2	29.6 ± 0.6

TABLE 4. White Blood Cell Population for Terminal Blood Samples.

	WBC differential count				
time	segs (%)	monos (%)	basos (%)	lymphs (%)	eos (%)
1 wk ($n = 5$)	35.3 ± 3.6	6.14 ± 5.0	0.68 ± 0.15	52.3 ± 5.2	3.1 ± 1.4
2 wk ($n = 5$)	36.4 ± 10.2	3.35 ± 1.8	0.50 ± 0.17	53.9 ± 11.4	4.8 ± 1.5
4 wk ($n = 5$)	35.1 ± 6.8	2.35 ± 0.64	0.48 ± 0.13	54.0 ± 6.6	6.0 ± 1.5
6 wk ($n = 5$)	31.4 ± 4.4	5.0 ± 2.9	0.45 ± 0.07	53.0 ± 6.3	9.2 ± 1.5
8 wk ($n = 5$)	34.6 ± 6.3	4.4 ± 1.2	0.83 ± 0.21	53.3 ± 5.6	5.7 ± 1.9
10 wk ($n = 5$)	42.2 ± 15.1	10.8 ± 6.9	0.70 ± 0.01	39.0 ± 6.8	7.0 ± 7.3

pected, the HCC core remains unchanged by the attachment of the PEG (Figure 3a,b). UV−vis provides the simplest technique for measuring the concentration of PEG-HCCs in a sample, although what is measured is the absorbance of the carbon core of the nanovector. Throughout this paper, all concentrations are given in terms of the concentration of the carbon core. Thermogravimetric analysis (TGA), Fourier transform infrared spectroscopy (FTIR), and X-ray photoelectron spectroscopy (XPS) all support the presence of PEG in the PEG-HCCs (Figure 3c−e). TGA indicates that the PEG-HCCs have a weight loss of 97%, while the HCCs have a weight loss of 58%. From these data, it can be calculated that the PEG-HCCs are 94% PEG by weight and that about 1 in 14 HCC carbons bears a PEG chain. The FTIR spectrum for the PEG-HCCs is very similar to the IR trace of PEG alone because the PEG-HCCs contain a large excess of the PEG repeat unit ($-CH_2CH_2O-$) relative to the HCC core. Nevertheless, a contribution from the HCCs is evident in the small set of peaks near 1750 nm. The XPS spectra for the PEG-HCCs are also dominated by the signal from the PEG, the C−O signal at 286 eV, while the spectra for the HCCs illustrate that the carbon core has been highly oxidized (peaks from 286 to 289 eV), but the major bond type is still carbon−carbon (284.5 eV). Because the PEG component of the PEG-HCCs dominates the XPS and FTIR measurements, it is not possible with these techniques to detect the amide bonds that would confirm the covalent attachment of the PEG to the HCCs.

Toxicity of PEG-HCCs. *In vivo* toxicity studies were conducted with PEG-HCCs. Nude mice (3 mice per group) were administered a single, tail-vein injection of PEG-HCCs (200 μL) at a concentration of either 200, 500, or 1000 mg/L (concentration is determined for the core of the HCC using UV−vis). After a single-dose injection, all of the mice were observed daily for 5 days, and none of the mice visually exhibited any signs of acute toxicities. After 5 days, the mice were euthanized, a terminal blood sample was collected, and the major organs including the heart, lungs, spleen, kidneys, liver, and brain were removed and examined for toxicity. At all tested concentrations, no abnormalities were seen in any of the organs, warranting a longer-term toxicity experiment.

PEG-HCCs at a concentration of 200 mg/L were investigated for longer-term toxicity experiments. Nude mice (5 groups of 5 mice) received a 200 μL by tail-vein injection of PEG-HCCs once per week, for up to 10 weeks. Note that, for therapeutic drug delivery, PEG-HCCs were administered weekly at half of this dose (100 mg/L) for only 3 weeks. All animals were observed daily; the mice did not show any visual signs of fatigue or discomfort and slowly increased in body weight over the 10 week period (Figure 4a). In addition to daily visual assessment of all animals, major organs and blood analyses were also assessed at necropsy. A group of 5 mice was randomly selected and euthanized after 1, 2, 4, 6, 8, and 10 weeks of weekly treatments. Major organs including the heart, lungs, spleen, kidneys, liver, and brain were removed, formalin-fixed, and examined for toxicity under light microscopy. For all mice examined, no toxicity was apparent in any of the organs analyzed (images of liver, spleen, and kidneys from weeks 1 and 10 are presented in Figure 4b). It was difficult to examine the lungs for toxicity, due to an error in sample preparation for histology. Dark spots were seen in Kupfer (macrophage) cells in the liver, but besides the macrophage, the organ appeared normal (Figure 4c). The dark spots are likely carbonaceous aggregates formed from the PEG-HCCs.

When each group of mice was euthanized, a terminal blood sample was taken from each mouse for standard chemistry by our animal core laboratory. All of the indicators of liver function analyzed were within normal limits (aspartate aminotransferase (AST), alanine aminotransferase (ALT), alkaline phosphatase (ALK PHOS) and, bilirubin). Blood, urea, nitrogen (BUN), and serum creatinine levels are indicative of kidney function and were found to be within normal limits (Table 1). Electrolytes potassium, sodium, and chloride were found to be within normal limits, as were glucose as a measure of metabolism and calcium as an indicator of cardiac and bone health (Table 2). Regression analysis found no trends over time for the levels of AST, ALT, creatine, sodium, potassium, and glucose. While ALK PHOS, bilirubin, BUN, chloride, and calcium remained within normal ranges, correlation with linear changes over time were found (Table S1 in Supporting Information). White blood cells (WBC), red blood cells (RBC), and platelets were also maintained within normal limits. Hemoglobin, hematocrit, mean corpuscular volume (MCV), mean corpuscular hemoglobin (MCH), and mean corpuscular hemoglobin concentration (MCHC) as secondary measures of RBC health were found to be at normal levels (Table 3). The composition of the WBC population also remained within normal ranges during the 10 weeks (Table 4). While they remained within normal ranges, a correlation with a linear change over time was found for WBC, platelet count, hemoglobin, hematocrit, MCV, MCH, segs, monos, basos, and eos. No trends were found for RBC, MCHC, and lymphs (Table S1).

Drug Loading. PEG-HCCs were loaded with PTX by dropwise addition of PTX in methanol (5 mg in 1 mL) to a rapidly stirring solution of PEG-HCCs in water (100 mg/L concentration of core HCCs, 5 mL). The solution was bath-sonicated, concentrated to 3 mL by rotary evaporation to remove the methanol, and then diluted back to the original volume (5 mL) with water, providing a translucent solution of PTX noncovalently associated with PEG-HCCs (PTX/PEG-HCCs) (Figure 5a). The efficacy of the loading is easy to monitor, as PTX is insoluble in water. If too much PTX is added, a precipi-

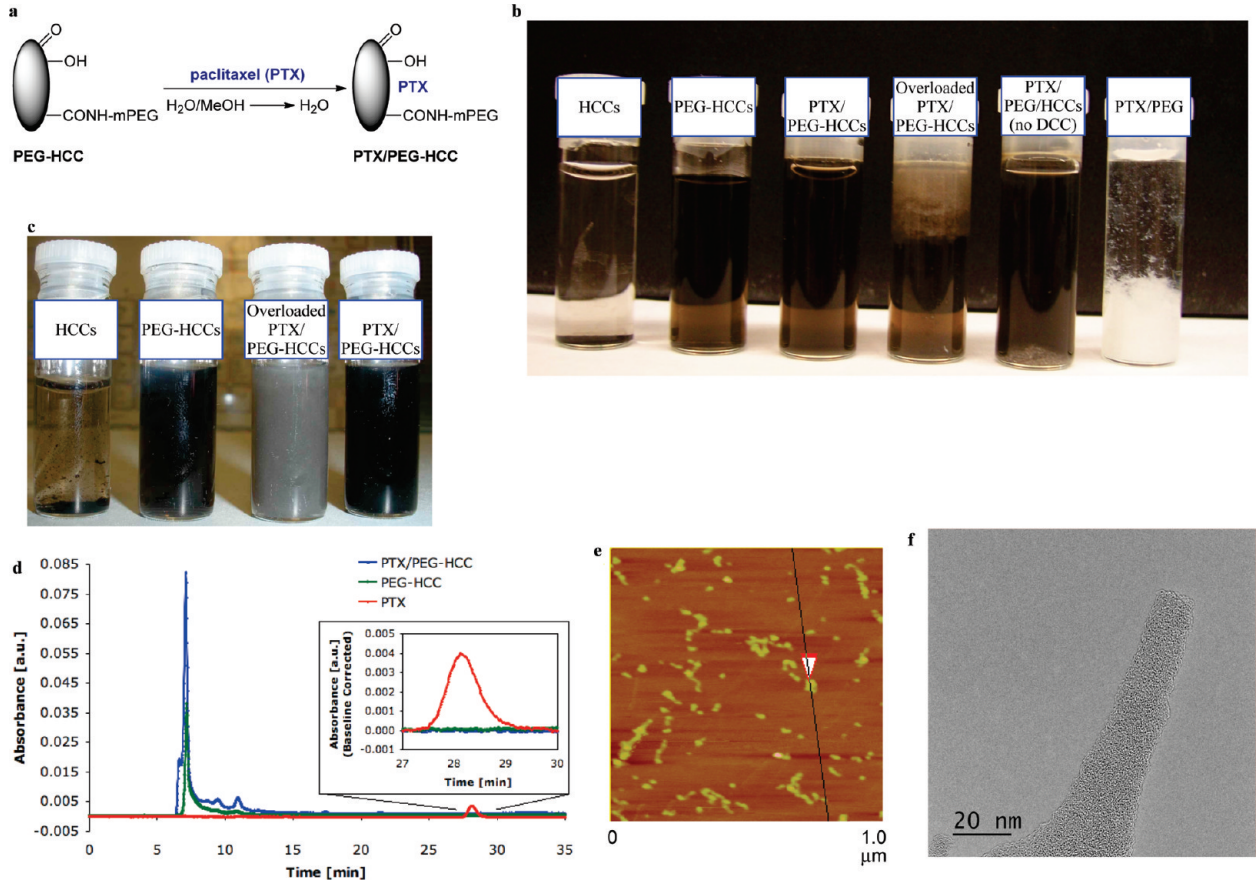

Figure 5. Loading of PEG-HCCs with PTX. (a) PTX in methanol was slowly added to the PEG-HCCs, and the methanol was removed. (b) Water solutions following centrifugation of, in order from left to right, HCCs (dispersible but insoluble and shown at the bottom of the vial), PEG-HCCs, 1 mg/mL PTX loaded in PEG-HCCs, 3 mg/mL PTX loaded in PEG-HCCs, 1 mg/mL PTX loaded in PEG mixed with HCCs (no covalent attachment of the PEG to the HCCs; note the white PTX precipitate at the bottom of the vial), and 1 mg/mL PTX loaded in PEG. (c) PBS solutions after 5 min of, in order from left to right, HCCs (insoluble), PEG-HCCs, 3 mg/mL PTX loaded in PEG-HCCs, and 1 mg/mL PTX loaded in PEG-HCCs. If these samples are allowed to stand for 7 days, a black precipitate settles out of both the PEG-HCCs and PTX/PEG-HCCs. However, shaking the sample completely redisperses the material. (d) Stacked HPLC traces of PTX/PEG-HCCs, PEG-HCCs, and free PTX. (e) AFM image of aggregated PTX/PEG-HCCs on mica. The overlapping red arrows indicate where the height of the PEG-HCCs was measured to be 4.7 nm. (f) TEM image of PTX/PEG-HCCs projecting over an empty domain on a lacy carbon grid. The PTX/PEG-HCCs have aggregated during the sample preparation, which consisted of placing an aqueous solution of PTX/PEG-HCCs on the lacy carbon grid and drying the sample at 70 °C for 16 h.

tate is observed (Figure 5b,c). Indeed, if no PEG-HCCs are used, the PTX immediately precipitates upon addition to the water. By simple visual inspection, it was determined that it is possible to load the PEG-HCCs with up to 1.6 mg/mL of PTX.[39] A loading of 1 mg/mL was used for all studies so that solubility would not be a concern. Using a size exclusion column, high-performance liquid chromotography analysis (HPLC) confirmed that at this loading all of the PTX was sequestered by the PEG-HCCs (Figure 5d). Free PTX (1 mg/mL) is observed at 28.1 min in this HPLC analysis, while free PEG-HCCs (100 mg/L) give a tailing peak with a maximum at 7.2 min. When the two are combined, no peak for the free PTX is observed and the PEG-HCC peak alters shape. The ζ-potential of PTX/PEG-HCCs was −37.82 mV, a marked difference from PEG-HCCs that is indicative of an interaction between the HCCs and the PTX. In addition, while the AFM of PTX/PEG-HCCs is visually similar to PEG-HCCs, the height of the particles is increased, again suggesting that the PTX is interacting with them (Figure 5e). TEM images of the PTX/PEG-HCCs were very similar to those obtained for the PEG-HCCs and HCCs (Figure 5f). It is likely that the PTX is being sequestered on the hydrophobic domains of the HCC core of each PEG-HCC. If the loading protocol is followed, but PEG alone is used instead of PEG-HCCs, nearly all of the PTX precipitates (Figure 5b). If the HCCs are simply mixed with mPEG-NH_2, the PEG noncovalently wraps the HCCs and is observed by FTIR and XPS following purification. However, the material is unable to sequester PTX at a concentration of 1 mg/mL (Figure 5b), likely because the hydrophobic interaction between the PTX and the HCCs cannot occur without disrupting the noncovalent binding between the PEG and the HCCs.

***In Vitro* Efficacy.** Two head and neck cancer cell lines (OSC-19, SqCC/Y1) and two breast cancer cell lines (A549, H1975) were treated for 3 days with PTX/PEG-HCCs, PEG-HCCs, and the commercial formulation

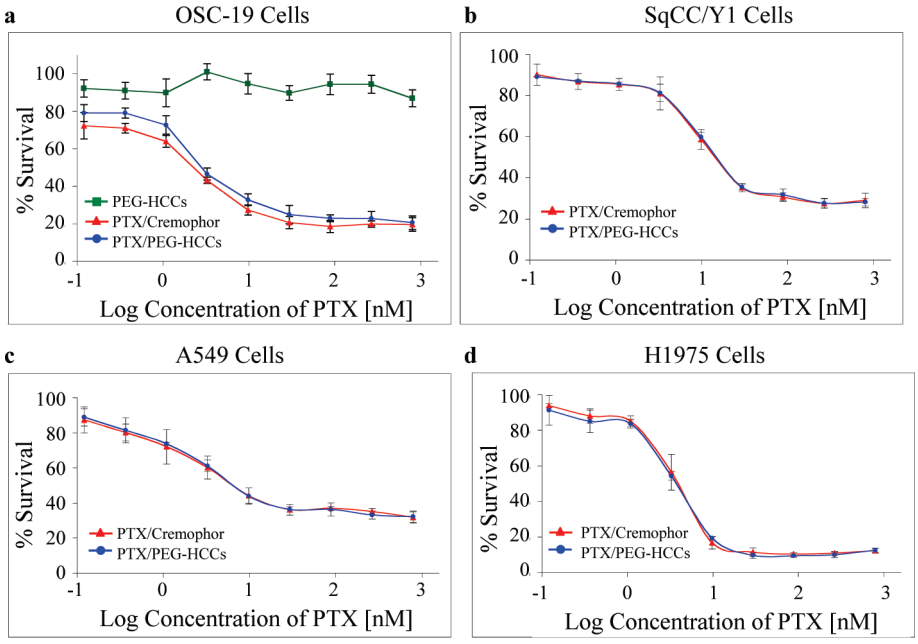

e

Cell Type	A549	OSC-19	SqCC/Y1	H1975
PTX/Cremophor IC_{50} [nM]	1.77±0.37	1.94±0.11	2.88±0.43	1.69±1.00
PTX/PEG-HCCs IC_{50} [nM]	1.69±0.31	1.87±0.06	2.68±0.53	1.63±0.97

Figure 6. ***In vitro*** **efficacy of PTX/PEG-HCCs. Treatment of two head and neck cancer cell lines (a,b) and two breast cancer cell lines (c,d) with PTX/PEG-HCCs (blue line with circles) and PTX/Cremophor (red line with triangles). Plot (a) also shows the inability of PEG-HCCs alone to kill cells (green line with squares). Each graph represents an individual trial. Error bars are standard errors. Table (e) presents the IC_{50} data for an average of three trials and the standard deviations.**

Taxol, which is PTX/Cremophor. Subsequently, an MTT assay was performed to assess cell survival for the different concentrations of each compound. The PTX/PEG-HCCs were prepared such that the highest concentration of PTX used in the *in vitro* assay (500 nM) corresponded to a PEG-HCCs concentration of 3.6 mg/L. Duplicate trials with OSC-19 cells demonstrated that the PEG-HCCs have no toxicity at concentrations of the carbon core less than 4 mg/L (Figure 6a, green line with squares). For all cell lines studied, the assay was performed in triplicate, and the cell-killing efficacy of the PTX/PEG-HCCs treatment and that of the PTX/Cremophor treatment was nearly equivalent (Figure 6a−d). The efficacy of both treatments varied slightly based on the confluency of the cells. Thus, graphs are provided for individual trials. However, in order to capture the range of variation introduced by the confluency, Figure 6e presents the averages of all three runs; note that in each case the IC_{50} values for treating with PTX/PEG-HCCs or PTX/Cremophor are equivalent within the margins of error. A noncancerous keratinocyte cell line, HOK16B, was also treated, and again, the PEG-HCCs had no effect while the PTX/PEG-HCCs and the PTX/Cremophor were equally effective (Figure S1 in Supporting Information).

The stability of the PTX/PEG-HCCs formulation was evaluated over a 20 week period (Table 5). Samples of PTX/PEG-HCCs and PTX/Cremophor were prepared and stored at 23 and 4 °C, respectively. New OSC-19 cells were treated with each solution at each week indicated in the table. There was a small amount of week to week variation in the efficacy of both samples, likely due to the slightly different confluency of the cells week to week. This is supported by the fact that, whenever the IC_{50} rose or fell for one sample, it also did so for the other sample. Indeed, in all cases, the PTX/PEG-HCCs formulation was as effective as the PTX/Cremophor and no decline in the potency of either sample was observed over the 20 weeks.

In Vivo **Efficacy.** Following the *in vitro* work, we proceeded to evaluate the effectiveness of PTX/PEG-HCCs treatment on an orthotopic murine model of oral squamous cell carcinoma using the OSC-19 cell line (Figure 7). OSC-19 cells were injected into the tongues of 32 mice as described previously.[40] After 12 days, the mice were randomized into four groups and treated weekly with either a saline solution (control, $n = 9$), PTX/Cremophor ($n = 9$), PTX/PEG-HCCs ($n = 9$), or PEG-HCCs ($n = 5$). For each of the PTX formulations, the dose was 8 mg of PTX/kg. The PEG-HCCs were used at a concentration of 100 mg/L. The tumor sizes were measured twice

TABLE 5. Stability of the PTX/PEG-HCCs Evaluated in Comparison to PTX/Cremophor over Time

	IC_{50} for OSC19 cells (nM)							
treatment	wk 1	wk 2	wk 3	wk 4	wk 5	wk 6	wk 7	wk 20
PTX/PEG-HCCs	2.04	1.94	1.62	4.08	1.57	2.09	2.98	3.00
PTX/Cremophor	1.95	1.84	1.34	3.94	1.45	1.97	2.72	2.95

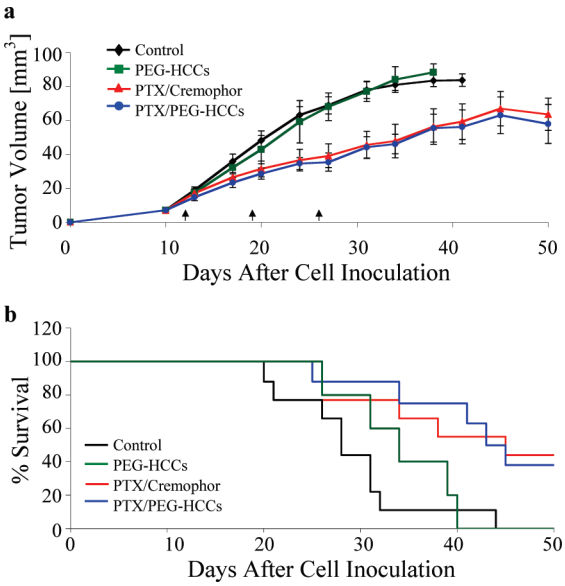

Figure 7. Treatment of tumors in an orthotopic murine model of oral squamous cell carcinoma. Mice with orthotopically established oral tongue tumors were injected once weekly (at days 12, 19, and 26) with the treatment (control, PTX/Cremophor, PTX/PEG-HCCs, PEG-HCCs). (a) Tumor volume measured twice weekly. Error bars are standard errors. A paired Student's *t* test was used to compare the differences in tumor volume. The three arrows along the *x*-axis denote the 3 days of treatment injections. (b) Animal survival over 50 days. Survival was analyzed by the Kaplan−Meier method and compared with log-rank tests.

per week using microcalipers. The mice were also weighed twice per week. The mice were euthanized using carbon dioxide asphyxiation if they lost more than 20% of their preinjection body weight or became moribund. The remaining mice were euthanized at 50 days postcell inoculation. The PTX/Cremophor and PTX/PEG-HCCs statistically significantly decreased tumor volume and increased survival relative to the control treatment; the two PTX treatments were statistically indistinguishable from each other. Mice treated with PTX/Cremophor or PTX/PEG-HCCs also had similar body weights (Figure S2 in Supporting Information).

Biodistribution of PEG-HCCs and PTX/PEG-HCCs. Having demonstrated *in vivo* efficacy, we sought to determine the biodistribution in both healthy and orthotopically implanted tumor mice of the PTX/PEG-HCCs and, for comparison, the PEG-HCCs. In order to track the nanovectors, they were labeled with ^{111}In, which has a half-life of 2.8 days.[41,42] The ^{111}In was attached to the HCCs *via* chelation with diethylenetriaminepentaaceticacid (DTPA) groups at the ends of the PEG chains (Figure 8). In order to prepare these functionalized PEG chains, DTPA isothiocyanate was coupled to an amino, azido functionalized PEG oligomer. The resulting product was joined to an amino, alkynyl functionalized 6000 MW PEG chain using click chemistry.[43] Treatment with Na_2S and $Ca(OH)_2$ removed any Cu bound to the DTPA.[44] The conjoined polymer was then coupled to the HCCs using standard peptide coupling conditions, and small molecule contaminants were removed using a size exclusion column. The purified DTPA-PEG-HCCs were mixed with ^{111}In, and any unbound ^{111}In was removed by a second size exclusion column to yield [^{111}In]DTPA-PEG-HCCs. To demonstrate that the ^{111}In was tightly bound to the DTPA-PEG-HCCs, the binding was challenged with ethylenediaminetetraaceticacid (EDTA). When exposed to an excess of EDTA, 93% of the ^{111}In remained bound to the DTPA-PEG-HCCs. In comparison, when ^{111}In was mixed with PEG-HCCs and challenged with EDTA, only 19% remained bound. This confirmed that the indium was strongly bound by the DTPA chelate. To provide a control for biodistribution studies, DTPA-PEG-NH_2 was acylated to yield DTPA-PEG-Ac that was loaded with ^{111}In as described above.

In order to determine the biodistribution, 27 nude mice were administered 200 μL of [^{111}In]DTPA-PEG-HCCs (0.14 μM concentration of PEG, a concentration equivalent to that of the PEG in the other samples), PTX/[^{111}In]DTPA-PEG-HCCs, or [^{111}In]DTPA-PEG-Ac, at a HCC concentration of 200 mg/L *via* tail-vein injections. Three mice were euthanized at each of the following time points: 0 (no treatment control), 0.5, 1, 3, 6, 18, 24, 48, 72, and 96 h, and a terminal blood sample was taken along with the heart, lungs, spleen, kidneys, liver, brain, and tongue, and the radioactivity of each sample was determined using a gamma counter. Data for the blood, kidneys, liver, spleen, and lungs are presented in Figure 9. [^{111}In]DTPA-PEG-HCCs accumulate in the spleen, liver, and kidneys in comparison to the [^{111}In]DTPA-PEG control that accumulates in the kidneys. This is very similar to other nanovectors.[16,41,42,45] It is interesting to note that the PTX/PEG-HCCs are highly distributed in the lungs relative to the PEG-HCCs. High distribution to the lungs has been seen for Taxol,[46] which suggests that the PTX is interacting with the PEG-HCCs and altering their distribution. Data for the heart, tongue, and brain are presented in the Supporting Information as there was little distribution to these organs (Figure S3). There was no accumulation of any of the samples in the brain. The urine and feces were collected every 24 h; a significant fraction of all three samples were shown to be quickly excreted through the urine and a smaller amount in the feces (Figure S3). This excretion signal could also come from the small fraction of weakly bound indium.

The same biodistribution study was performed using an orthotopic tongue tumor mouse model. The 30 mice were injected with 3×10^5 OSC-19 head and neck cancer cells one week prior to injection of [^{111}In]DTPA-PEG-Ac, [^{111}In]DTPA-PEG-HCCs, or PTX/[^{111}In]DTPA-PEG-HCCs. Within 7 days, a tumor was visible on the tongue of each mouse. The rest of the biodistribution study was performed in the same manner as for healthy mice. The biodistribution of [^{111}In]DTPA-PEG-HCCs and PTX/[^{111}In]DTPA-PEG-HCCs is very similar to that in the healthy mice with accumulation in the liver, spleen,

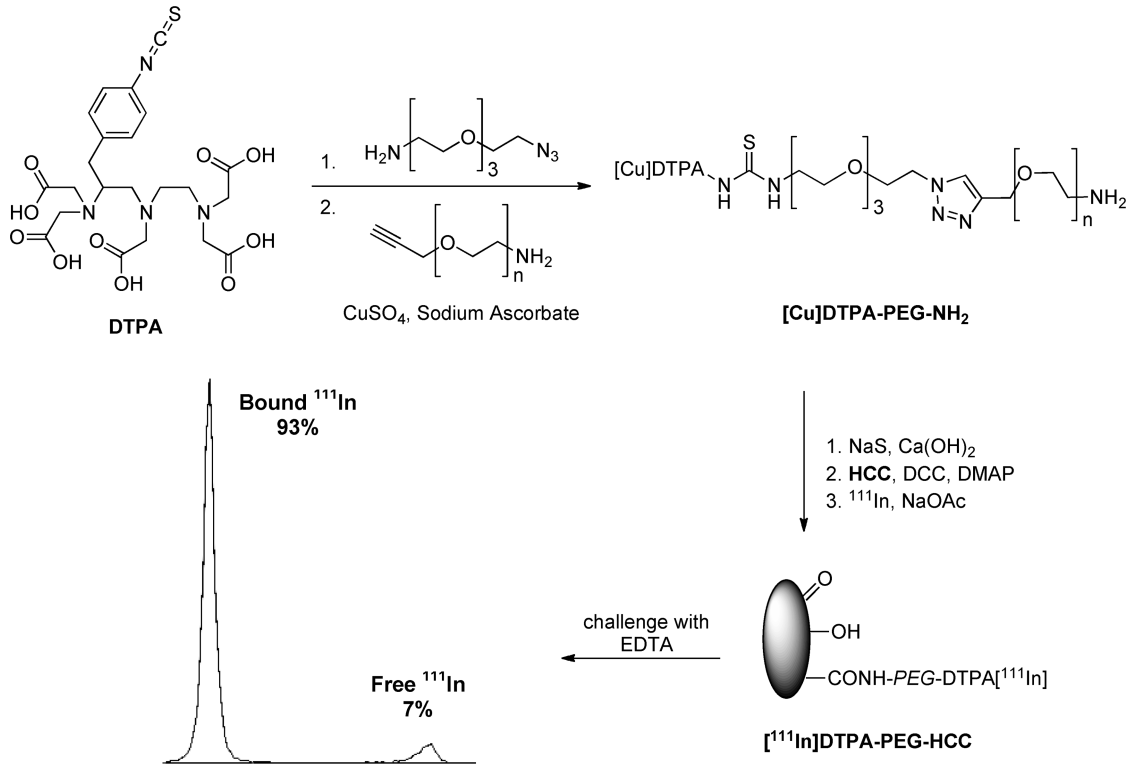

Figure 8. Synthesis of [^{111}In]DTPA-PEG-HCCs and subsequent challenge with EDTA, which confirmed the strong binding of most of the indium.

and kidneys (Figure 10). The PTX/[^{111}In]DTPA-PEG-HCC also accumulates in the lungs, as expected from the earlier results. In addition, the [^{111}In]DTPA-PEG-HCCs and PTX/[^{111}In]DTPA-PEG-HCCs reach the tumor on the tongue. As for the healthy mice, there was little distribution to the heart, tongue, and brain (Figure S4 in Supporting Information). There was no accumulation of any of the samples in the brain. The urine and feces were collected every 24 h; a significant fraction of all three samples were shown to be quickly excreted through the urine and a smaller amount in the feces (Figure S4).

CONCLUSION

We have demonstrated that a carbon nanomaterial (PEG-HCCs) can be an effective nanovector drug delivery platform, both *in vitro* and *in vivo*, when noncovalently loaded with an unmodified drug (PTX). Preliminary toxicity studies indicated that the PEG-HCCs themselves are not acutely toxic, even when given weekly. The PTX/PEG-HCCs formulation proved to be stable and as effective as Taxol (PTX/Cremophor) both *in vitro* and *in vivo*. Biodistribution studies demonstrated that, similar to other nanoparticles, both PTX/PEG-HCCs and PEG-HCCs reach the tumor but primarily accumulate in the liver and spleen. While preparing a novel nanovector drug delivery platform that is as effective as a commercial formulation is noteworthy, in the future, it will be essential to develop a targeted PEG-HCCs formulation that improves upon current clinical formulations.

METHODS

Synthesis of HCCs. SWCNTs were purified following a reported protocol.[36] **Caution!** *This process uses a highly reactive mixture of acids; strong exothermic reactions are possible. Extreme caution should be used during the procedure. All oxidation reactions should be done in a fume hood, and appropriate safety equipment should be worn, including a lab coat, rubber smock, thick rubber gloves, safety glasses, and a full face and neck shield.* The purified SWCNTs (250 mg) were dissolved in oleum (125 mL) in a three-neck, 1 L round-bottomed flask with all joints sealed with Teflon and stirred for 5 days to disentangle them. The solution was then cooled to 0 °C with an ice bath, and an ice cold 1:1 mixture of oleum and nitric acid (62.5 mL/62.5 mL) was added in 20 mL portions. During the addition of this mixture, the temperature of the solution was monitored to ensure that it never exceeded 60 °C. When 60 °C was reached, the mixture was allowed to cool until the temperature returned to 10 °C before adding the next portion. The addition process took approximately 1 h. The final proportion of oleum/nitric acid was 3:1. When the addition of the acidic mixture was complete, the ice bath was removed and the solution was heated to 65 °C and stirred for 90 min. The solution was then cooled to room temperature and carefully poured onto ice (400 mL) to quench the reaction. The resulting solution was stirred for 16 h then filtered through a PTFE membrane (0.45 μm pore size). The handling of the material during this filtration is critical to obtain readily dispersible HCCs. During this filtration, the solid is constantly kept moist by the addition of water whenever the solid is nearly exposed. The pH of the liquid coming through the filter is checked until it reaches pH 6. At this point, the addition of water is terminated and all of the liquid is removed by filtration, but the solid still remains moist. Methanol

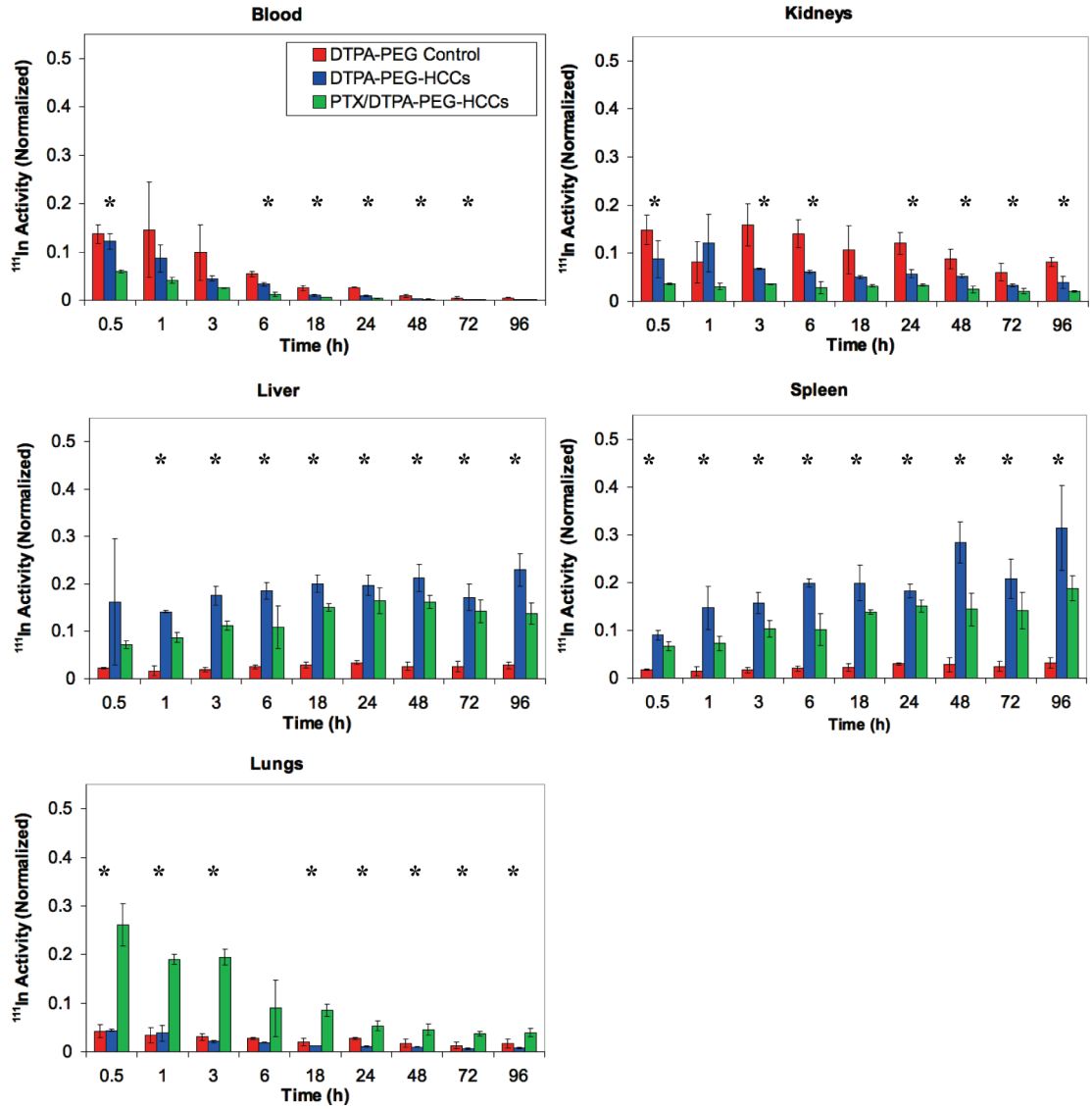

Figure 9. Distribution of [^{111}In]DTPA-PEG-Ac, [^{111}In]DTPA-PEG-HCCs, and PTX/[^{111}In]DTPA-PEG-HCCs in the blood, kidneys, liver, spleen, and lungs of healthy nude mice. The *y*-axis in all panels was normalized to the total organ radioactivity count divided by the organ's weight. This value is then divided by the initial radioactivity count injected in each mouse. All plots have the same *y*-axis scale to ease comparisons. *ANOVA is statistically significant ($p < 0.05$).

(150 mL) is slowly added to dissolve the solid, then ether (500 mL) is added to precipitate the solid and the liquid is removed by filtration, during which it is best to agitate the solid with a Teflon spatula. The final evaporation of the ether was done by placing the moist HCCs in a 50 mL beaker and using a hot plate, slowly allowing the HCCs to heat while continually pulverizing them with a Teflon spatula resulting in a fine, dry powder that was dried in a vacuum desiccator for 12 h to yield 112 mg of HCCs.

Synthesis of PEG-HCCs. HCCs (25 mg, 2.08 mmol of carbon) were added to DMF (25 mL), and the mixture was sonicated using a bath sonicator for 30 min, at which point all of the HCCs were dissolved. DCC (172 mg, 0.835 mmol) was added, and the reaction was stirred for 30 min with mPEG-NH_2 (208 mg, 0.042 mmol). DMAP (2 flakes) was added, and the reaction was stirred for 24 h. The solution was purified by dialysis in DMF and then water (50 000 MW cutoff dialysis bag, Membrane Filtration Products, Inc. Cat# 1-5050-34), followed by passage through a PD-10 column (GE Healthcare) to furnish 60 mL of PEG-HCCs with a carbon core concentration of 392 mg/L.

Loading PEG-HCCs with PTX. Paclitaxel dissolved in methanol (5 mg in 1 mL) was added dropwise into a rapidly stirring solution of PEG-HCCs in deionized water (5 mL, 100 mg/L concentration of core HCC). The mixture was stirred for 30 min, using a bath sonicator for 30 min, at which time, the solution was translucent and brown/black. To remove most of the methanol, the solution was concentrated on a rotovap at 70 °C to 3 mL. After concentration, the PTX/PEG-HCCs solution remained translucent. Note that, if precipitation is observed, then the sample is ruined and should be discarded. Finally, the solution was diluted back to the original volume (5 mL) with DI water to give a final PTX concentration of 1 mg/mL.

Images of Different Formulations. For the image of the samples in water, samples were placed in a 1/2 dram vial and centrifuged for 1 min at 3000 rpm. For the image of the samples in PBS, aqueous solutions of HCCs, PEG-HCCs, overloaded PTX/PEG-HCCs, and PTX/PEG-HCCs were combined 9:1 with 10× PBS to provide 1× PBS solutions. The samples were allowed to sit for 15 min before the picture was taken.

Characterization. TEM imaging was performed on a JEOL 2100. Samples were prepared from aqueous solutions of the nanomaterials that were then dropped onto 300 mesh holey lacey carbon grids on a copper support (Ted Pella, Inc.) and dried at 70 °C for 16 h. The hydrodynamic diameter of each nanomaterial was characterized through dynamic light scattering (Brookhaven, ZetaPALS with BI-9000AT digital autocorrelator, λ

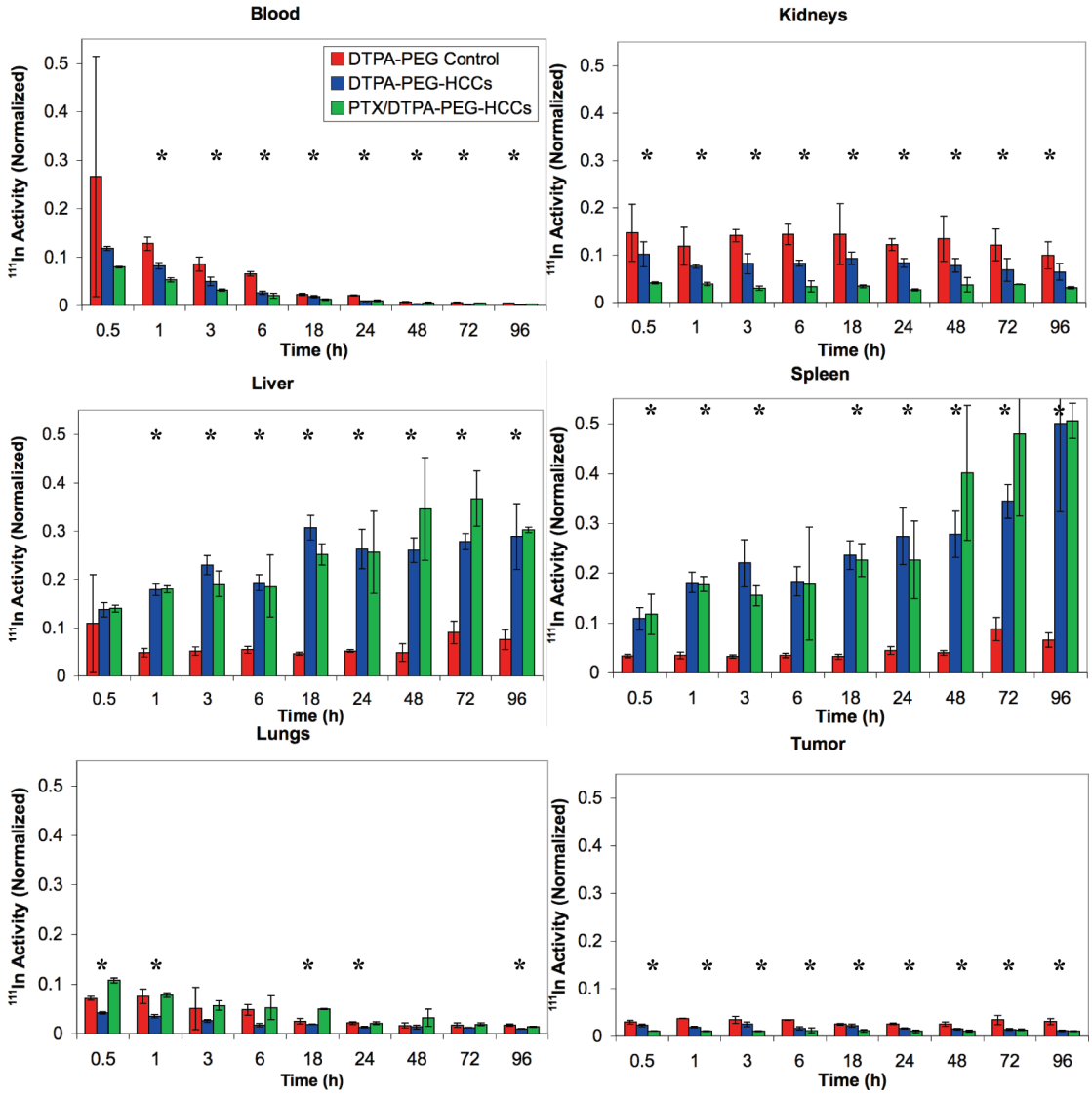

Figure 10. Distribution of [^{111}In]DTPA-PEG-Ac, [^{111}In]DTPA-PEG-HCCs, and PTX/[^{111}In]DTPA-PEG-HCCs in the blood, kidneys, liver, spleen, lungs, and tumor of tongue tumor burdened nude mice. The *y*-axis in all panels was normalized to the total organ radioactivity count divided by the organ's weight. This value is then divided by the initial radioactivity count injected in each mouse. All plots have the same *y*-axis scale to ease comparisons. *ANOVA is statistically significant ($p < 0.05$).

= 656 nm). The electrophoretic mobility of these aggregates was measured by phase analysis light scattering (PALS) using the ZetaPALS setup. A dip-in (Uzgiris type) electrode system with 4 mL polystyrene cuvettes was used, and measurements were taken at 20 °C. Static light scattering experiments were carried out using a Wyatt HELEOS II detector operating in batch mode. The system was calibrated with toluene and normalized using a 5 mg/mL solution of polystyrene in toluene. Samples were measured in 20 mL glass scintillation vials, and a baseline was defined by a vial containing pure solvent (either H_2O or a pH 14 aqueous solution). Particle sizes were extracted by a Zimm fit of the data. TGA was obtained on Q50 TA Instrument, using argon from room temperature to 950 at 10 °C/min rate. UV data were collected from a Shidmadzu UV-3101 PC and samples contained in 1 mL quartz cuvettes. Samples were dissolved in deionized water. The carbon core concentration of each sample was determined by the absorbance at 763 nm using the experimentally determined extinction coefficient of 0.0104 L/mg.[47] FTIR spectra were recorded using a Nicolet FTIR microscope with ATR objective. Raman spectra were obtained on a Renishaw Raman scope using a 633 nm HeNe laser. XPS experiments were performed on a PHI Quantera SXM scanning X-ray microprobe with 26.00 eV passing energy, 45° takeoff angle, and a 100 μm beam size. AFM was done using a Nanoscope IIIa (Digital Instrtument/Veeco Metrology) under tapping mode, scan rate of 1 Hz, and a resolution of 512 × 512 was used to record AFM images. Si tips n-doped with 1−10 Ωcm phosphorus, Veeco, MPP-11100-140 were also used. Samples were prepared by spin coating aqueous solutions of HCC and PEG-HCC at 3000 rpm for 10 min on top of mica surface (Ted Pella) and then rinsing with isopropyl alcohol. HPLC analysis was performed using a Waters 2695 separations module with a Waters 2487 dual λ absorbance detector, and the reading obtained at 254 nm was used. A Phenomex BioSep-SEC-S 2000 column was used. A flow of 0.8 mL/min was used for the eluent, which was 100% water from 0−15 min, then linearly ramped to 30% water/70% methanol at 25 min and linearly ramped back to 100% water at 35 min.

Toxicity Studies. ***Animal Care:*** BALB/c (nu/nu) mice were used under an animal protocol approved by the Institutional Animal Care and Use Committee at The University of Texas M.D. Anderson Cancer Center, which is accredited by the Association for the Assessment and Accreditation of Laboratory Animal Care, International (AAALAC). The mice were kept in sterile ventilated microisolators with corncob bedding and offered Harlan, Teklad Irradiated Diet # 2919 and reverse osmosis water. The mice were free of the following pathogens based on sentinel testing: mouse

parvo virus (MPV), minute virus of mice (MVM), Theiler's virus (GD7), epidemic diarrhea of infant mice (EDIM), pneumonia virus of mice (PVM), reovirus 3 (REO3), mouse adenovirus (MAD), K-virus (K), polyoma virus (poly), *Mycoplasma pulmonis* (M. pul), mouse hepatitis virus (MHV), ectromelia virus, lymphocytic choriomeningitis virus (LCMV), intestinal parasites, and ectoparasites. For the portion of the study where urine and feces were collected, the mice were kept in sterile metabolism cages and offered autoclaved reverse osmosis water and irradiated diet.

Optical Microscopy of Organs: Each organ was excised and fixed with 10% formalin in phosphate buffer saline (pH 7.4) and processed by embedding in paraffin. For organ histology, sections of each organ were taken and placed on glass slides and stained using hematoxylin and eosin. Evaluation of each sample was done by a board certified veterinary pathologist using an optical microscope (Olympus BX61, Center Valley, PA).

Chemistry and Hematology Analysis: Blood chemistry tests were performed with a Roche COBAS INEGRA 400 plus and software version 3.4.4.0809 and complete blood counts with a Simerns BayerAdvia 120 Hematology 69 analyzer. Both tests were completed by MD Anderson Animal Pathology Core Laboratory (CCSG−CA016672).

Short-Term Toxicity of PEG-HCCs in Healthy Mice: Fifteen BALB/c (nu/nu) mice were randomized into 3 mice per group for each PEG-HCC concentration (200, 500, and 1000 mg/L) and one control group which received saline. Each group received a tail-vein injection of 200 μL of PEG-HCCs or saline. The mice were visually monitored for 5 days. After 5 days, the mice were euthanized using CO_2. A terminal blood sample was collected and sent for pathology work. Various organs were also harvested (including heart, liver, lungs, kidneys, spleen, and brain) and placed in formalin for histopathological work.

Longer-Term Toxicity of PEG-HCCs in Healthy Mice: Thirty BALB/c (nu/nu) mice were randomized into 5 mice per group for each time point (1, 2, 4, 6, 8, 10 wk). Each group received a tail-vein injection of 200 μL of PEG-HCCs once per week until euthanization. The mice were weighed daily. The mice were euthanized using CO_2. A terminal blood sample was collected and analyzed. Various organs were also harvested (including heart, liver, lungs, kidneys, spleen, and brain) and placed in formalin for histology.

Effect of Treatment on the *In Vitro* Growth of Squamous Cancer Cells. ***General:*** The OSC-19 line was obtained from the Laboratory of Dr. Faye Johnson at M.D. Anderson Cancer Center. This cell line was established in Japan from a metastatic tumor to a cervical lymph node of a patient with well-differentiated SCC of the tongue.[48] This cell line was grown *in vitro* in Dulbecco's modified Eagle's medium (DMEM) supplemented with 10% fetal bovine serum (FBS), L-glutamine, sodium pyruvate, nonessential amino acids, and a 2-fold vitamin solution (Life Technologies, Inc., Grand Island, NY). The SqCC/Y1 human HNSCC line was obtained from the Laboratory of Dr. Vali Papadimitrakopoulou at M.D. Anderson Cancer Center. The H1975 human lung adenocarcinoma cell line was obtained from the Laboratory of Dr. John Heymach at M.D. Anderson Cancer Center. The A549 human nonsmall cell lung cancer was obtained from American Type Culture Collection (Rockville, MD). H1975 cells and A549 cells were maintained in RPMI 1640 containing penicillin−streptomycin (Flow Laboratories, Rockville, MD), nonessential amino acids, sodium pyruvate, L-glutamine, and 10% fetal bovine serum (FBS). The SqCC/Y1 cells were maintained in DMEM/F12 low glucose containing penicillin−streptomycin, L-glutamine, and 10% FBS. Adherent monolayer cultures were maintained on plastic and incubated at 37 °C in 5% CO_2 and 95% air. The cultures were free of *Mycoplasma* species and were maintained for no longer than 12 weeks after recovery from frozen stocks.

MTT Assay: Cells were grown for 24 h in a 96-well plate (2000 cells/well in 100 μL of 10% serum containing media) at 37 °C in 5% CO_2 and 95% air before treating with drugs. Serial dilutions of known PTX concentrations (500.0, 166.7, 55.6, 18.5, 6.17, 2.06, 0.69, 0.23, 0.08 nM) were prepared in media from each of the initial drug stock solutions (PTX/PEG-HCCs {PTX 1 mg/mL, PEG-HCCs 100 mg/L}, PEG-HCCs {PEG-HCCs 100 mg/L}, and PTX/Cremophor EL {PTX 6 mg/mL}). For each sample, 100 μL of each dilution was added to six wells. The cells were incubated for 3 days at 37 °C, then MTT solution (25 μL of 2 mg/mL) was added in each well. After incubation for 2 h, the media were removed by careful aspiration to avoid suctioning of the cells. Then, 100 μL of DMSO was added to each well in order to lyse the cells and solubilize the colored crystals. Finally, the plates were analyzed using an ELISA plate reader at a wavelength of 570 nm to measure optical density (OD) of each well, which proportionate to number of viable cells in each well. The percent of viable cells relative to control was obtained by dividing the average OD for the treated wells by the OD for the control wells.

Stability Assay: A PTX/PEG-HCCs solution was stored at room temperature, while a PTX/Cremophor (Taxol) solution was stored in the refrigerator at 4 °C. For each week indicated, an MTT assay was performed using new OSC-19 cells and the PTX/PEG-HCCs and PTX/Cremophor solutions.

In Vivo* Tumor Treatment.** ***Animals and Maintenance: Male athymic nude mice, age 8 to 12 weeks, were purchased from the animal production area of the National Cancer Institute−Frederick Cancer Research and Development Center (Frederick, MD). The mice were housed and maintained in laminar flow cabinets under specific pathogen-free conditions in facilities approved by the American Association for Accreditation of Laboratory Animal Care in accordance with current regulations and standards of the U.S. Department of Agriculture, the U.S. Department of Health and Human Services, and the National Institutes of Health. The mice were used in accordance with the Animal Care and Use Guidelines of the University of Texas M.D. Anderson Cancer Center (Houston, TX) under a protocol approved by the Institutional Animal Care Use Committee. The tumor sizes were measured with microcalipers. Tumor volume (V) was calculated using the formula $V = AB^2\pi/6$ (A, the longest dimension of the tumor and, B, the dimension of the tumor perpendicular to A).

In Vivo Experiments: Thirty-six athymic nude mice were injected in the tongue with 5×10^4 squamous cell carcinoma OSC-19 cells suspended in serum-free DMEM, as described previously.[40] Twelve days after the injection, tumor size was measured and all of the mice had similar sized tumors. The mice were randomized into four groups. Treatments (PBS as a placebo {$n = 9$}, PTX/PEG-HCCs {PTX 1 mg/mL, PEG-HCCs 100 mg/L, $n = 9$}, PTX/Cremophor EL {PTX 1 mg/mL, $n = 9$}, PEG-HCCs {PEG-HCCs 100 mg/L, $n = 5$}) were administered intravenously on days 12, 19, and 26 following cell injection by injecting 200 μL into the tail veins of the mice. The mice were examined twice a week for tumor size and weight loss. The mice were euthanized using carbon dioxide asphyxiation if they lost more than 20% of their pre-injection body weight or became moribund. The remaining mice were euthanized at 50 days postcell inoculation.

Synthesis of [^{111}In]DTPA-PEG-HCCs. ***Synthesis of Amino, Alkynyl Functionalized PEG:*** A tube that could be sealed was oven-dried, fitted with a septa, and pump/filled three times. THF (10 mL) and potassium bis(trimethylsilyl)amide (2.22 mL, 1.11 mmol) were added, and the solution was cooled to −78 °C. In a graduated cylinder fitted with a septa, ethylene oxide (5 mL, 100 mmol) was condensed at −78 °C in the presence of CaH_2 (250 mg) and canula transferred to the reaction tube. The septum on the reaction tube was removed, and the tube was quickly sealed. The reaction was stirred at 60 °C for 48 h. The reaction was cooled to room temperature, and allyl bromide (278 μL, 25 mmol) was added. The tube was resealed, and the reaction was stirred at 45 °C for 24 h. The solution was cooled to room temperature and transferred to a sepratory funnel. Water (30 mL) was added, and the solution was extracted with $CHCl_3$. The combined $CHCl_3$ extracts were dried with $MgSO_4$, filtered to remove the $MgSO_4$, and concentrated to 10 mL. Et_2O was added, precipitating the polymer, which was recrystallized from EtOH and dried to yield 3.6 g of amino, alkynyl functionalized PEG. GPC analysis indicated that the polymer had a MW of 5900 and a PDI of 1.32. ^{1}H NMR (400 MHz, CDCl3, ppm): δ 4.21 (d, 2H J = 2.4 Hz), 3.75−3.54 (m), 2.45 (t, 1H, J = 2.4 Hz).

Synthesis of DTPA-PEG-NH$_2$: p-SCN-Bn-DTPA (donated by Macrocyclics, http://www.macrocyclics.com, 0.059 g, 0.099 mmol) was dissolved in 2 mL of anhydrous DMF. To this was added 11-azido-2,6,9-trioxaundecan-1-amine (0.022 g, 0.099 mmol). The solution was allowed to stir under nitrogen for 12 h, followed by removal of DMF under vacuum to yield DTPA-PEG. DTPA-PEG (0.080 g, 0.160 mmol) was dissolved in water (8 mL) and *tert*-

butanol (8 mL). To this was added amino, alkynyl functionalized PEG (6000 MW, 0.628 g, 0.106 mmol). It was slowly heated using a heat gun until the solid dissolved. To this was added copper sulfate (0.027 g, 0.106 mmol), and the solution quickly turned blue in color. This was followed by addition of sodium ascorbate (0.021 g, 0.106 mmol). The blue color persisted after addition of sodium ascrobate, suggesting that the DTPA was chelating the copper. The solution was then transferred to a 10 000 MWCO dialysis bag and placed in continuous flow DI water for 24 h. The copper was then removed by addition of sodium sulfide (0.025 mL, 0.106 mmol). The solution quickly turned brown in color; this was followed by addition of calcium hydroxide (0.008 g, 0.106 mmol). The mixture was allowed to stir for 1 h, and the insoluble copper was removed by filtration. The same procedure (addition of sodium sulfide followed by addition of calcium hydroxide) was repeated a second time, and the filtrate was almost colorless, suggesting complete removal of copper. The water was removed under vacuum. The light-yellow-colored solid was redissolved in a minimal amount of chloroform (5 mL), and the solution was added dropwise to cold ether (50 mL). The mixture was placed in the freezer for 1 h and then filtered, providing DTPA-PEG-NH_2 as a white solid, MALDI-TOF MS using a sinapinic acid matrix *m/z* calcd for H + $C_{30}H_{46}N_8O_{13}S$ 759, found 759.

Synthesis of DTPA-PEG-HCCs: HCCs (18 mg, 1.50 mmol of carbon) were added to DMF (20 mL), and the mixture was sonicated using a bath sonicator for 30 min, at which point all of the HCCs were dissolved. DCC (310 mg, 1.50 mmol) was added, and the reaction was stirred for 30 min. DTPA-PEG-NH_2 (100 mg, 0.015 mmol) and DMAP (2 flakes) were added, and the reaction was stirred for 24 h. The solution was purified by dialysis in DMF for 1 day and then water for 5 days (50 000 MW cutoff dialysis bag, Membrane Filtration Products, Inc. Cat# 1-5050-34), followed by passage through a PD-10 column (GE Healthcare).

Synthesis of ^{111}In-DTPA-PEG-HCCs: DTPA-PEG-HCCs (6 mL, 200 mg/L of HCC core) were placed in a small vial. To this was added ^{111}In (130 μCi) in 200 μL sodium acetate (0.1 M). The solution was vortexed for 1 min and then allowed to stand for 20 min before passage through a PD-10 column. The [^{111}In]DTPA-PEG-HCCs were then diluted with saline to a concentration of 200 mg/L of HCC core.

EDTA Challenge of ^{111}In Binding to PEG-HCCs or DTPA-PEG-HCCs: PEG-HCCs or DTPA-PEG-HCCs (100 μL) were placed in a vial. To this was added ^{111}In (160 μCi) in an aqueous solution of sodium acetate (0.1 M). The solution was vortexed and then allowed to stand for 30 min before passage through a PD-10 column. The solutions obtained were analyzed for ^{111}In binding using instant TLC. The instant TLC strips were developed with PBS (pH 7.4) containing 4 mM EDTA and quantified using a Bioscan IAR-2000 TLC Imaging Scanner (Bioscan). Free ^{111}In moved to the solvent front (R_f = 0.9), and the [^{111}In]-DTPA-PEG-HCCs remained at the original spot (R_f = 0.0).

Preparation of PTX/^{111}In-PEG-HCCs: To a vigorously stirring solution of ^{111}In-PEG-HCCs (10 mL, 200 mg/L) in a round-bottom flask was added dropwise PTX (10 mg) in methanol (MeOH, 1 mL). The solution was allowed to stir for 10 min and was then bath sonicated for 2 h. The volume was then reduced to 9 mL using a heat gun while the solution was stirring to remove the MeOH. The solution was then reconstituted to 10 mL with 10× PBS, resulting in a solution of 1 mg/mL PTX and an HCC concentration of 200 mg/L.

Biodistribution Studies. ***Biodistribution in Healthy Mice:*** For each material, 30 BALB/c (nu/nu) mice were randomized to be used over the following 10 time points (3 mice per time point): 0.5, 1, 3, 6, 18, 24, 48, 72, 96, and 120 h. Each animal received a single i.v. injection (200 μL) of the material being studied in that group, either [^{111}In]DTPA-PEG-Ac (0.14 μM concentration of PEG, a concentration equivalent to that of the PEG in the other samples), [^{111}In]DTPA-PEG-HCC (200 mg/L concentration of HCC core), or PTX/[^{111}In]DPTA-PEG-HCC (200 mg/L concentration of HCC core) dissolved in 1× PBS. After injection, each animal was placed in a plastic metabolism cage in order to collect the urine and feces. The animals were fed a Teklad irradiated diet #2919 and water *ad libitum*. For each group and time point, three animals were euthanized and terminal blood samples were collected and various organs harvested (heart, liver, lungs, kidneys, spleen, brain, and tongue) and placed into preweighed scintillation vials. Each organ and blood sample was weighed and analyzed for ^{111}In activity using a gamma counter. Total voided urine and excreted feces were collected every 24 h and analyzed for ^{111}In activity.

Biodistribution in Orthotopic Squamous Cell Cancer Mouse Model: The same method was used as was used for healthy mice, except that 7 days prior to treatment, each mouse was anesthetized using 45 mg/kg Nembutal and 5×10^5 OSC-19 cells were injected on the tongue of each animal. After the 7 days, the tumor was visible.

Acknowledgment. We thank Z. Sun for the TEM images, J. Yu for DLS and ζ-potential measurements, R. Verduzco for SLS measurements, K. Mohamedali for assistance with HPLC analysis, the Alliance for NanoHealth through a subcontract from the University of Texas Health Science Center, Houston (Department of Defense: W8XWH-07-2-0101); the Traumatic Brain Injury Consortium, funded by the United States Army; the Nanoscale Science and Engineering Initiative of the National Science Foundation under NSF Award EEC-0647452 for funding through the NSF Center for Biological and Environmental Nanotechnology; The University of Texas MD Anderson PANTHEON Program; NIH Cancer Center Support Grant CA16672; MD Anderson Support Grant (CA016672). The DTPA isothiocyanate was kindly provided by Garry Kiefer at Macrocyclics, Inc.

Supporting Information Available: AFM and XPS for the PEG-HCCs and HCCs, experimental procedures for each figure, and complete cell and animal information are available. This material is available free of charge *via* the Internet at http://pubs.acs.org.

REFERENCES AND NOTES

1. O'Driscoll, C. M.; Griffin, B. T. Biopharmaceutical Challenges Associated with Drugs with Low Aqueous Solubility—The Potential Impact of Lipid-Based Formulations. *Adv. Drug Delivery Rev.* **2008**, *60*, 617–624.
2. Stinchcombe, T. E. Nanoparticle Albumin-Bound Paclitaxel: A Novel Cremphor-EL®-Free Formulation of Paclitaxel. *Nanomedicine* **2007**, *2*, 415–423.
3. Gradishar, W. J.; Tjulandin, S.; Davidson, N.; Shaw, H.; Desai, N.; Bhar, P.; Hawkins, M.; O'Shaughnessy, J. Phase III Trial of Nanoparticle Albumin-Bound Paclitaxel Compared with Polyethylated Castor Oil-Based Paclitaxel in Women with Breast Cancer. *J. Clin. Oncol.* **2005**, *23*, 7794–7803.
4. Gursoy, N.; Garrigue, J. S.; Razafindratsita, A.; Lambert, G.; Benita, S. Excipient Effects on *In Vitro* Cytotoxicity of a Novel Paclitaxel Self-Emulsifying Drug Delivery System. *J. Pharm. Sci.* **2003**, *92*, 2411–2418.
5. Chen, H.; Zhang, Z.; McNulty, C.; Olbert, C.; Yoon, H. J.; Lee, J. W.; Kim, S. C.; Seo, M. H.; Oh, H. S.; Lemmo, A. V.; *et al.* A High-Throughput Combinatorial Approach for the Discovery of a Cremophor EL-Free Paclitaxel Formulation. *Pharm. Res.* **2003**, *20*, 1302–1308.
6. Crosasso, P.; Ceruti, M.; Brusa, P.; Arpicco, S.; Dosio, F.; Cattel, L. Preparation, Characterization and Properties of Sterically Stabilized Paclitaxel-Containing Liposomes. *J. Controlled Release* **2000**, *63*, 19–30.
7. Shuai, X. T.; Merdan, T.; Schaper, A. K.; Xi, F.; Kissel, T. Core-Cross-Linked Polymeric Micelles as Paclitaxel Carriers. *Bioconjugate Chem.* **2004**, *15*, 441–448.
8. Ruan, G.; Feng, S.-S. Preparation and Characterization of Poly(lactic acid)-Poly(ethylene glycol)-Poly(lactic acid) (PLA-PEG-PLA) Microspheres for Controlled Release of Paclitaxel. *Biomaterials* **2003**, *24*, 5037–5044.
9. Riehemann, K.; Schneider, S. W.; Luger, T. A.; Godin, B.; Ferrari, M.; Fuchs, H. Nanomedicine—Challenge and Perspectives. *Angew. Chem., Int. Ed.* **2009**, *48*, 872–897.
10. Ferrari, M. Cancer Nanotechnology: Opportunities and Challenges. *Nat. Rev. Cancer* **2005**, *5*, 161–171.
11. Lee, C. C.; MacKay, J. A.; Fréchet, J. M. J.; Szoka, F. C. Designing Dendrimers for Biological Applications. *Nat. Biotechnol.* **2005**, *23*, 1517–1526.
12. Kostarelos, K.; Bianco, A.; Prato, M. Promises, Facts and Challenges for Carbon Nanotubes in Imaging and Therapeutics. *Nat. Nanotechnol.* **2009**, *4*, 627–633.

13. Wu, H.-C.; Chang, X.; Liu, L.; Zhao, F.; Zhao, Y. Chemistry of Carbon Nanotubes in Biomedical Applications. *J. Mater. Chem.* **2010**, *20*, 1036–1052.
14. Yinghuai, A.; Peng, A. T.; Carpenter, K.; Maguire, J. A.; Hosmane, N. S.; Takagaki, M. Substituted Carborane-Appended Water-Soluble Single-Wall Carbon Nanotubes: New Approach to Boron Neutron Capture Therapy Drug Delivery. *J. Am. Chem. Soc.* **2005**, *127*, 9875–9880.
15. Bhirde, A. A.; Patel, V.; Gavard, J.; Zhang, G.; Sousa, A. A.; Masedunskas, A.; Leapman, R. D.; Weigert, R.; Gutkind, J. S.; Rusling, J. F. Targeted Killing of Cancer Cells *In Vivo* and *In Vitro* with EGF-Directed Carbon Nanotube-Based Drug Delivery. *ACS Nano* **2009**, *3*, 307–316.
16. Chen, J.; Chen, S.; Zhao, X.; Kuznetsova, L. V.; Wong, S. S.; Ojima, I. Functionalized Single-Walled Carbon Nanotubes as Rationally Designed Vehicles for Tumor-Targeted Drug Delivery. *J. Am. Chem. Soc.* **2008**, *130*, 16778–16785.
17. Liu, Z.; Chen, K.; Davis, C.; Sherlock, S.; Cao, Q.; Chen, X.; Dai, H. Drug Delivery with Carbon Nanotubes for *In Vivo* Cancer Treatment. *Cancer Res.* **2008**, *68*, 6652–6660.
18. Jesorka, A.; Orwar, O. Liposomes: Technologies and Analytical Applications. *Annu. Rev. Anal. Chem.* **2008**, *1*, 801–832.
19. Harrington, K. J.; Lewanski, C. R.; Northcote, A. D.; Whittaker, J.; Wellbank, H.; Vile, R. G.; Peters, A. M.; Stewart, J. S. W. Phase I−II Study of Pegylated Liposomal Cisplatin (SPI-077^{TM}) in Patients with Inoperable Head and Neck Cancer. *Ann. Oncol.* **2001**, *12*, 493–496.
20. Zhang, X.; Meng, L.; Lu, Q.; Fei, Z.; Dyson, P. J. Targeted Delivery and Controlled Release of Doxorubicin to Cancer Cells Using Modified Single Wall Carbon Nanotubes. *Biomaterials* **2009**, *30*, 6041–6047.
21. Heister, E.; Neves, V.; Tilmaciu, C.; Lipert, K.; Beltran, V. S.; Coley, H. M.; Silva, S. R. P.; McFadden, J. Triple Functionalisation of Single-Walled Carbon Nanotubes with Doxorubicin, a Monoclonal Antibody, and a Fluorescent Marker for Targeted Cancer Therapy. *Carbon* **2009**, *47*, 2152–2160.
22. Sun, X.; Liu, Z.; Welsher, K.; Robinson, J. T.; Goodwin, A.; Zaric, S.; Dai, H. Nano-Graphene Oxide for Cellular Imaging and Drug Delivery. *Nano Res.* **2008**, *1*, 203–212.
23. Liu, Z.; Robinson, J. T.; Sun, X.; Dai, H. PEGylated Nanographene Oxide for Delivery of Water-Insoluble Cancer Drugs. *J. Am. Chem. Soc.* **2008**, *130*, 10876–10877.
24. Ali-Boucetta, H.; Al-Jamal, K. T.; McCarthy, D.; Prato, M.; Bianco, A.; Kostarelos, K. Multiwalled Carbon Nanotube−Doxorubicin Supramolecular Complexes for Cancer Therapeutics. *Chem. Commun.* **2008**, 459–461.
25. Liu, Z.; Sun, X.; Nakayama-Ratchford, N.; Dai, H. Supramolecular Chemistry on Water-Soluble Carbon Nanotubes for Drug Loading and Delivery. *ACS Nano* **2007**, *1*, 50–56.
26. Partha, R.; Mitchell, L. R.; Lyon, J. L.; Joshi, P. P.; Conyers, J. L. Buckysomes: Fullerene-Based Nanocarriers for Hydrophobic Molecule Delivery. *ACS Nano* **2008**, *2*, 1950–1958.
27. Lay, C. L.; Liu, H. Q.; Tan, H. R.; Liu, Y. Delivery of Paclitaxel by Physically Loading onto Poly(ethylene glycol) (PEG)-Graft-Carbon Nanotubes for Potent Cancer Therapeutics. *Nanotechnology* **2010**, *21*, 065101.
28. Guo, L.; Liu, X.; Sanchez, V.; Vaslet, C.; Kane, A. B.; Hurt, R. H. A Window of Opportunity: Designing Carbon Nanomaterials for Environmental Safety and Health. *Mater. Sci. Forum* **2007**, *544−545*, 511−516.
29. Drezek, R. A.; Tour, J. M. Is Nanotechnology Too Broad to Practise? *Nat. Nanotechnol.* **2010**, *5*, 168–169.
30. Hurt, R.; Monthioux, M.; Kane, A. Toxicology of Carbon Nanomaterials: Status, Trends, and Perspectives on the Special Issue. *Carbon* **2006**, *44*, 1028–1033.
31. Liu, Z.; Davis, C.; Cai, W.; He, L.; Chen, X.; Dai, H. Circulation and Long-Term Fate of Functionalized, Biocompatible Single-Walled Carbon Nanotubes in Mice Probed by Raman Spectroscopy. *Proc. Natl. Acad. Sci. U.S.A.* **2008**, *105*, 1410–1415.
32. Schipper, M. L.; Nakayama-Ratchford, N.; Davis, C. R.; Kam, N. W.; Chu, P. S.; Liu, Z.; Sun, X. M.; Dai, H. G.; Gambhir, S. S. A Pilot Toxicology Study of Single-Walled Carbon Nanotubes in a Small Sample of Mice. *Nat. Nanotechnol.* **2008**, *3*, 216–221.
33. Kolosnjaj-Tabi, J.; Hartman, K. B.; Boudjemaa, S.; Ananta, J. S.; Morgant, G.; Szwarc, H.; Wilson, L. J.; Moussa, F. *In Vivo* Behavior of Large Doses of Ultrashort and Full-Length Single-Walled Carbon Nanotubes after Oral and Intraperitoneal Administration to Swiss Mice. *ACS Nano* **2010**, *4*, 1481–1492.
34. Liu, X.; Hurt, R. H.; Kane, A. B. Biodurability of Single-Walled Carbon Nanotubes Depends on Surface Functionalization. *Carbon* **2010**, *48*, 1961–1969.
35. Chen, Z.; Kobashi, K.; Rauwald, U.; Booker, R.; Fan, H.; Hwang, W.-F.; Tour, J. M. Soluble Ultra-Short Single-Walled Carbon Nanotubes. *J. Am. Chem. Soc.* **2006**, *128*, 10568–10571.
36. Price, B. K.; Lomeda, J. R.; Tour, J. M. Aggressively Oxidized Ultra-Short Single-Walled Carbon Nanotubes Having Oxidized Sidewalls. *Chem. Mater.* **2009**, *21*, 3917–3923.
37. Duque, J. G.; Parra-Vasquez, A. N. G.; Behabtu, N.; Green, M. J.; Higginbotham, A. L.; Price, B. K.; Leonard, A. D.; Schmidt, H. K.; Lounis, B.; Tour, J. M.; *et al.* Diameter-Dependent Solubility of Single-Walled Carbon Nanotubes. *ACS Nano* **2010**, *4*, 3063–3072.
38. Stephenson, J. J.; Hudson, J. L.; Leonard, A. D.; Price, B. P.; Tour, J. M. Repetitive Functionalization of Water-Soluble Single-Walled Carbon Nanotubes. Addition of Acid-Sensitive Addends. *Chem. Mater.* **2007**, *19*, 3491–3498.
39. Recently, we have developed a different preparation that makes use of increased equivalents of PEG and DCC to synthesize the PEG-HCCs that allows up to 12 mg/mL of PTX to be sequestered. This improved synthesis was developed after the initiation of the *in vitro* and *in vivo* experiments described, so the higher-loaded nanovectors were not used.
40. Myers, J. N.; Holsinger, F. C.; Jasser, S. A.; Bekele, B. N.; Fidler, I. J. An Orthotopic Nude Mouse Model of Oral Tongue Squamous Cell Carcinoma. *Clin. Cancer Res.* **2002**, *8*, 293–298.
41. Liu, Z.; Cai, W.; He, L.; Nakayama, N.; Chen, K.; Sun, X.; Chen, X.; Dai, H. *In Vivo* Biodistribution and Highly Efficient Tumour Targeting of Carbon Nanotubes in Mice. *Nat. Nanotechnol.* **2007**, *2*, 47–52.
42. Villa, C. H.; McDevitt, M. R.; Escorcia, F. E.; Rey, D. A.; Bergkvist, M.; Batt, C. A.; Scheinberg, D. A. Synthesis and Biodistribution of Oligonucleotide-Functionalized, Tumor-Targetable Carbon Nanotubes. *Nano Lett.* **2008**, *8*, 4221–4228.
43. van Dijk, M.; Rijkers, D. T. S.; Liskamp, R. M. J.; van Nostrum, C. F.; Hennink, W. E. Synthesis and Applications of Biomedical and Pharmaceutical Polymers *via* Click Chemistry Methodologies. *Bioconjugate Chem.* **2009**, *20*, 2001–2016.
44. Hong, P. K. A.; Li, C.; Banerji, S. K.; Wang, Y. Feasibility of Metal Recovery from Soil Using DTPA and Its Biostability. *J. Hazard. Mater.* **2002**, *94*, 253–272.
45. Kang, B.; Yu, D.; Dai, Y.; Chang, S.; Chen, D.; Ding, Y. Biodistribution and Accumulation of Intravenously Administered Carbon Nanotubes in Mice Probed by Raman Spectroscopy and Fluorescent Labeling. *Carbon* **2009**, *47*, 1189–1192.
46. Wang, Y.; Li, Y.; Wang, Q.; Wu, J.; Fang, X. Pharmacokinetics and Biodistribution of Paclitaxel-Loaded Pluronic P105/L101 Mixed Polymeric Micelles. *J. Pharm. Soc. Jpn.* **2008**, *128*, 941–950.
47. Lucente-Shultz, R. M.; Moore, V. C.; Leonard, A. D.; Price, B. K.; Kosynkin, D. V.; Lu, M.; Partha, R.; Conyers, J. L.; Tour, J. M. Antioxidant Single-Walled Carbon Nanotubes. *J. Am. Chem. Soc.* **2009**, *131*, 3934–3941.
48. Yokoi, T.; Yamaguchi, A.; Odajima, T.; Furukawa, K. Establishment and Characterization of a Human Cell Line Derived From a Squamous Cell Carcinoma of the Tongue. *Tumor Res.* **1988**, *23*, 43–57.